Journal of Pharmacokinetics and Pharmacodynamics (2019) 46:89–101
https://doi.org/10.1007/s10928-019-09620-z

ORIGINAL PAPER

Indirect pharmacodynamic models for responses with circadian removal

Vivaswath S. Ayyar[1] · Wojciech Krzyzanski[1] · William J. Jusko[1]

Received: 11 December 2018 / Accepted: 17 January 2019 / Published online: 29 January 2019

Abstract

Rhythmicity in baseline responses over a 24-h period for an indirect pharmacological effect R(t) can arise from either a periodic time-dependent input rate $k_{in}(t)$ or a periodic time-dependent loss constant $k_{out}(t)$. If either $k_{in}(t)$ or $k_{out}(t)$ follows some nonstationary biological rhythm (e.g., circadian), then the response R(t) also displays a periodic behavior. Indirect response models assuming time-dependent input rates $[k_{in}(t)]$ have been utilized to capture drug effects on various physiological responses such as hormone suppression, immune cell trafficking, and gene expression in tissues. This paradigm was extended to consider responses with circadian-controlled loss $[k_{out}(t)]$ mechanisms. Theoretical equations describing this model are presented and simulations were performed to examine expected response behaviors. The model was able to capture the chronobiology and pharmacodynamics of applicable drug responses, including the uricosuric effects of lesinurad in humans, suppression of the beta amyloid (Aβ) peptide by a gamma-secretase inhibitor in mouse brain, and the modulation of extracellular dopamine by a dopamine transporter inhibitor in rat brain. This type of model has a mechanistic basis and shows utility for capturing drug responses displaying nonstationary baselines controlled by removal mechanism(s).

Keywords Circadian rhythm · Nonstationary baseline · Pharmacodynamics · Indirect response model · Periodic removal · Mathematical modeling

Introduction

Chronopharmacologic rhythms occurring within diverse physiological systems are common phenomena. Examples include body temperature, cardiovascular functioning, gastric acid secretion, secretion of hormones (melatonin, cortisol, growth hormone, prolactin), organ blood flows, renal filtration, enzymatic activities, plasma protein concentrations, and several others. Various underlying cellular and molecular mechanisms are "programmed in time" [1], giving rise to periodic behaviors under homeostasis, including circadian rhythms. Four basic Indirect Response Models (IDR) have been described [2] and applied to numerous drugs [3, 4]. The classical models assume zero-order production (k_{in}) and first-order loss (k_{out}) yielding a constant baseline of the response variable (R) over time. Time-dependent complexities in responses (e.g. circadian) can be accounted for by supplementing k_{in} or k_{out} with a time-dependent production or loss process of the response variable. While the basic model has been extended to account for circadian rates of production [5], consideration of time-dependent responses due to circadian loss mechanisms [i.e. $k_{out}(t)$] has not been assessed thus far.

It is well recognized in pharmacokinetics that the disposition of some exogenous compounds can be influenced by time-dependent mechanisms such as time-of-day variations in absorption, plasma protein binding and distribution, metabolism, and elimination [6]. For example, significant circadian variations were observed in the plasma concentrations of 5-fluorouracil (5-FU) in patients receiving a protracted continuous infusion at 300 mg/m^2/day [7]. In addition, circadian variations in the activity

Electronic supplementary material The online version of this article (https://doi.org/10.1007/s10928-019-09620-z) contains supplementary material, which is available to authorized users.

✉ William J. Jusko
wjjusko@buffalo.edu

[1] Department of Pharmaceutical Sciences, School of Pharmacy and Pharmaceutical Sciences, State University of New York at Buffalo, Buffalo, NY 14214, USA

of dihydropyrimidine dehydrogenase, the major catabolizing enzyme of 5-FU, was measured in peripheral blood mononuclear cells from the same patients. This rhythm shared an inverse relationship with the variation in plasma 5-FU [7]. Circadian variation in the hepatic elimination rate of 5-FU in isolated perfused rat liver has also been reported [8]. Similarly, it is expected that mediators controlling indirect responses or endogenous markers used in pharmacodynamic modeling can exhibit circadian variations arising from periodic removal mechanisms. Indeed, the circadian rhythms of endogenous substances, including plasma concentrations of body ions or electrolytes (e.g. sodium and potassium), nitrogenous waste products (e.g. urea nitrogen and uric acid), brain metabolites [e.g. amyloid beta (Aβ)], and neurotransmitters (e.g. dopamine and acetylcholine) occur through diverse underlying elimination processes.

The Aβ peptide is the main component of amyloid plaques, which are extracellular deposits found in the brains of patients with Alzheimer's disease. Circadian variations in hippocampal and striatal extracellular fluid Aβ concentrations in mice brain have been reported, with higher concentrations associated with wakefulness [9]. The Aβ is secreted upon proteolytic cleavage of the amyloid precursor protein by the beta and gamma secretases. Of current interest in drug development are molecules that inhibit the production of amyloid plaques (e.g. secretase inhibitors) [10, 11]. The glymphatic system clears metabolic waste from the brain, including Aβ [12], with the rate of removal significantly increased during sleep [13–15]. Previous modeling efforts in this area have not accounted for circadian variations in baseline Aβ while examining the PK/PD effects of drugs acting to alter this target.

Dopamine is a neurotransmitter released by dopaminergic neurons into synapses, extracellular fluid spaces within the brain, where upon binding the dopamine receptor on postsynaptic neurons, it can mediate signaling events related to motor control, motivation, arousal, reinforcement, and reward. Various psychotropic drugs (e.g. cocaine and phencyclidine) as well as therapeutic agents (e.g. methylphenidate and benztropines) act to modulate dopamine actions within the brain. Circadian rhythms in the extracellular concentrations of dopamine in various regions of the rodent and murine brain have been characterized [16–18]. Ferris et al. identified that circadian variation in dopamine tone did not relate to dopamine cell firing rate (i.e. production), but was governed by daily variations in the dopamine transporter activity mediating dopamine reuptake from the synaptic cleft (i.e. removal) [17].

Uric acid is the end product of an exogenous pool of purines and endogenous purine metabolism. Exogenous uric acid is derived from diet (e.g. animal meats) whereas endogenous production of uric acid is mainly from the liver. Almost all free uric acid is filtered through the kidney glomeruli, while 90% re-enters the circulation via transporter-mediated tubular reabsorption [19, 20]. Circadian rhythms in serum uric acid have been reported in human subjects [21, 22], with an apparent inverse relationship to circadian variations in glomerular filtration rate (GFR) [21, 23]. Hyperuricemia is central to the development of gout. Several compounds are being developed to treat hyperuricemia, including drugs targeting renal transporters of uric acid, mainly URAT1 and OAT4 [24].

The purpose of this report is to extend the theory and practice of indirect response modeling to consider circadian removal of the response variable. Mathematical derivation, simulations, and data fitting to applicable pharmacologic responses were employed to generate and apply new relationships for drugs with indirect mechanisms of action.

Theoretical

The two general indirect response models with periodic production rate or periodic loss are shown in Fig. 1. The differential equations for describing two possible

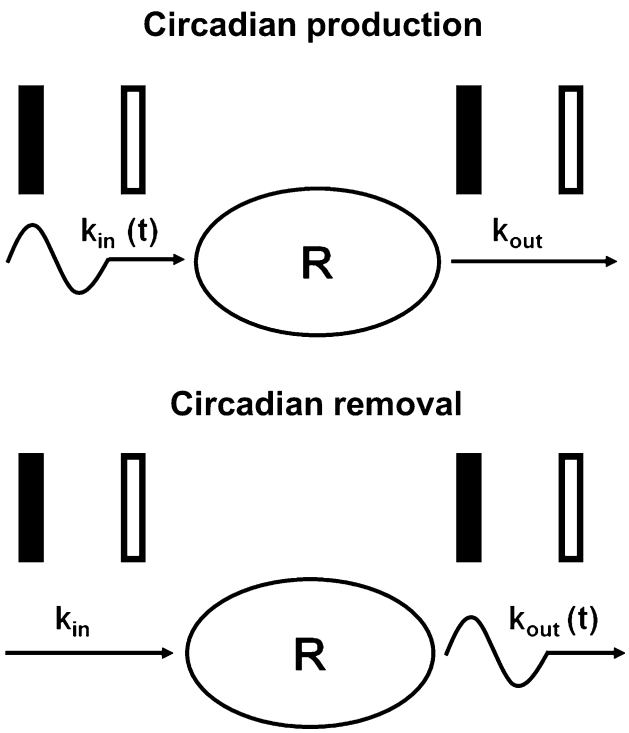

Fig. 1 Two General Indirect Response Models with Circadian Baselines. "R" represents the pharmacodynamic response variable. Solid arrows depict stationary rates of production or removal (k_{in} or k_{out}) whereas curved arrows depict periodic rates of production or removal [$k_{in}(t)$ or $k_{out}(t)$]. Solid boxes represent inhibition whereas open boxes depict stimulation

mechanisms producing circadian rhythms in baseline responses in the absence of drug are

$$\frac{dR_b}{dt} = k_{in}(t) - k_{out} \cdot R_b(t) \quad (1)$$

where $k_{in}(t)$ is a circadian function of time and k_{out} a first-order removal constant, and

$$\frac{dR_b}{dt} = k_{in} - k_{out}(t) \cdot R_b(t) \quad (2)$$

where $k_{out}(t)$ is a circadian function of time and k_{in} a zero-order production constant. The circadian baseline $R_b(t)$ can be described by the cosine function predicting symmetrical behavior

$$R_b(t) = R_m + R_a \cdot \cos\left(\frac{2\pi}{T} \cdot (t - t_p)\right) \quad (3)$$

where R_m is the mean baseline (mesor), R_a is the amplitude, t_p the peak time (acrophase), and T = 24 h (at $t = t_p$, $\cos(0) = 1, R_b(t_p) = R_m + R_a$; at $t = t_p \pm T/2$, $\cos(\pi) = -1$, $R_b(t_p \pm T/2) = R_m - R_a; R_m \geq R_a$) Equation 3 can be rearranged to express $k_{in}(t)$ as

$$k_{in}(t) = k_{out} \cdot R_b(t) + \frac{dR_b}{dt}(t) \quad (4)$$

and solved to yield an explicit function

$$k_{in}(t) = k_{out} \cdot R_m + k_{out} \cdot R_a \cdot \cos\left(\frac{2\pi}{T} \cdot (t - t_p)\right) - \frac{2\pi}{T} \cdot R_a \cdot \sin\left(\frac{2\pi}{T} \cdot (t - t_p)\right) \quad (5)$$

Similarly, Eq. 4 can be rearranged to express $k_{out}(t)$ as

$$k_{out}(t) = \frac{k_{in} - \frac{dR_b}{dt}(t)}{R_b(t)} \quad (6)$$

and solved to yield an explicit function

$$k_{out}(t) = \frac{k_{in} + \frac{2\pi}{T} \cdot R_a \cdot \sin\left(\frac{2\pi}{T} \cdot (t - t_p)\right)}{R_m + R_a \cdot \cos\left(\frac{2\pi}{T} \cdot (t - t_p)\right)} \quad (7)$$

Derivations for Eqs. (5) and (7) are presented in the Appendix.

Based upon the mechanism of action of the drug, the four classical IDR models depict inhibition (Models I and II) or stimulation (Models III and IV) of either production or loss of the response. Thus, the rate of the change of the response R with time for IDR model with either time-dependent production or loss can be described as:

$$\frac{dR}{dt} = k_{in}(t) \cdot (1 + H_1(t)) - k_{out} \cdot (1 + H_2(t)) \cdot R(t) \quad (8)$$

or

$$\frac{dR}{dt} = k_{in} \cdot (1 + H_1(t)) - k_{out}(t) \cdot (1 + H_2(t)) \cdot R(t) \quad (9)$$

where the pharmacologic processes operate according to capacity-limited functions:

$$\text{Model I} : H_1(t) = -\frac{I_{\max} \cdot C(t)}{IC_{50} + C(t)} \text{ and } H_2(t) = 0 \quad (10a)$$

$$\text{Model II} : H_1(t) = 0 \text{ and } H_2(t) = -\frac{I_{\max} \cdot C(t)}{IC_{50} + C(t)} \quad (10b)$$

$$\text{Model III} : H_1(t) = \frac{S_{\max} \cdot C(t)}{SC_{50} + C(t)} \text{ and } H_2(t) = 0 \quad (10c)$$

$$\text{Model IV} : H_1(t) = 0 \text{ and } H_2(t) = \frac{S_{\max} \cdot C(t)}{SC_{50} + C(t)} \quad (10d)$$

The initial condition is the baseline value at time $t = 0$

$$R(0) = R_m + R_a \cdot \cos\left(\frac{2\pi}{T} \cdot t_p\right) \quad (11)$$

Assumptions in the proposed models

In addition to the general assumptions associated with the four basic IDR models [4], these two circadian IDR models assume that rhythmicity in baseline responses are fully accounted for by either a nonstationary k_{in} or k_{out} process. An assumption is also made that the periodicity in baseline responses is described by a single cosine function. The applicability of other biorhythmic functions (e.g. dual ramps, dual zero-order) in capturing nonstationary production rates have been examined [5].

Methods

Data

The data utilized in this report were obtained from the literature. The mean values of the pharmacokinetic and pharmacodynamic (treatment and baseline response) data were extracted from published graphs by computer digitization (WebPlotDigitizer, version 4.1, https://automeris.io/WebPlotDigitizer). Thus, the estimated PK and PD parameters of the compounds studied should be considered approximate.

Data analysis

A sequential approach to modeling the PK and PD data was employed. Plasma or tissue drug concentrations were fitted to an appropriate compartmental PK model or

mathematical function to provide a reasonable characterization of the concentration–time data. In turn, the fitted drug concentrations were used to drive inhibition or stimulation functions acting on the turnover process (k_{in} or k_{out}) as mechanistically appropriate. Placebo and drug treatment data were fitted simultaneously to estimate drug-related pharmacodynamic parameters, k_{in} or k_{out}, and the cosine parameters describing $R_b(t)$. The ADAPT 5 software was used for all data fitting and simulation of model equations (see model code in Supplementary Materials) [25]. The maximum likelihood method was applied for fitting the data. The residual error variance model specified for PK and PD outputs was:

$$V_i = V(\theta, \sigma, t) = [\sigma_1 + \sigma_2 \cdot Y(\theta, t_i)]^2 \quad (12)$$

where V_i is the variance of the ith data point, σ_1 and σ_2 are the variance parameters, and Y_i is the model predicted concentration or response. Variance parameters σ_1 and σ_2 were estimated along with model parameters during fittings. The goodness-of-fit was assessed by visual inspection of the fitted curves, improvement in the log-likelihood objective function (− 2LL), examination of residuals, and precision (CV%) of the estimated parameters.

Results

Model simulations

To examine the expected behaviors of indirect response models for analysis of data obtained from systems with circadian responses, basic indirect response models with nonstationary production and removal were derived and used to generate the response data for a drug with mono-exponential kinetics with the elimination rate $k_{el} = 0.3\,\mathrm{h}^{-1}$ and five doses yielding initial concentrations of $C_0 = 10, 100, 1000, 10,000,$ and $100,000$ mg. The cosine parameters describing periodicity in baseline response were fixed to $R_m = 100$, $R_a = 20$, $T = 24$ h, and $t_p = 19$ h. The pharmacodynamic parameters were set up as: $I_{max} = 0.9$, $S_{max} = 10$, $IC_{50} = SC_{50} = 10$, and $k_{out} = 0.5\,\mathrm{h}^{-1}$ or $k_{in} = 52.5$ unit/h. The response data were generated with no relative standard deviation (noise).

The rhythmic profile of the baseline for an indirect pharmacodynamic response is equivalent upon using either a circadian production (Eq. 1) or circadian removal (Eq. 2) process (Fig. 2). Therefore, the two possible mechanisms cannot be discriminated based on baseline response data alone. The pharmacodynamic response profiles for each IDR model type for drugs administered at the mesor of the circadian baseline, described by Models I to IV, exhibited grossly similar profiles with changes in dose (Fig. 2), consistent with basic expectations of the classical IDR models. In addition to assessing the response profiles upon dosing at the mesor of circadian response (Fig. 2), the effect of time of dosing was examined by simulating the response profiles for each IDR model at the nadir and peak of the circadian baseline (Fig. S1A and S1B). In general, the extent of pharmacodynamic enhancement (or suppression) of the response at the three different points of dosing (nadir, mesor, and peak) is consistent with previous assessments on the role of baseline for indirect responses [26], with baseline values correlating with net pharmacodynamic response (i.e. the higher the baseline, the greater the AUC of response). While differences between the $k_{in}(t)$ and $k_{out}(t)$ models were minor regardless of dosing times, greater divergence between the simulated net responses for both model types were observed with dosing at higher baseline response values. Numerical differences between both circadian model types can be demonstrated based upon the distinct simulated model response versus time values generated by each model, as depicted for a single 10,000 mg dose given at the mesor (Table S1). Our simulations imply that model discrimination ($k_{in}(t)$ vs. $k_{out}(t)$) based on dose escalation might be practically infeasible. Shown in Fig. 3 is a single baseline response, which is produced by two distinct patterns of underlying circadian mechanisms ($k_{in}(t)$ vs. $k_{out}(t)$). Per the simulations in Figs. 2 and 3, a pharmacodynamic net response, for example, one described by IDR Model III, will be greatest when $k_{out}(t)$ is lowest, whereas the AUC of response would occur soon after $k_{in}(t)$ has reached a peak.

Amyloid-β suppression

Inhibitors and modulators of the gamma secretase enzyme in the brain are under development for the treatment of Alzheimer's disease. By decreasing the formation of long chain amyloid peptides such as $A\beta_{1–40}$ and $A\beta_{1–42}$, gamma secretase modulators (GSM) prevent the accumulation and aggregation of Aβ plaques in the brain. The glymphatic system clears metabolic waste from the brain, including Aβ, with the rate of removal significantly increased during sleep. The amount of Aβ in the brain extracellular space is governed by the amount produced by brain cells and removal by glial cells and convective flow (i.e. glymphatic processing) [12, 13].

Circadian fluctuations over two cycles (48 h) in ISF Aβ in the brain of 3-month-old APPswe/PS1δE9 mice was obtained from the literature [9]. Percent reductions in brain Aβ from baseline was assessed upon oral dosing of 30 and 100 mg/kg of an investigational GSM, BMS-869,780, in 3-month-old 3 × Tg mice [27]. Animals in both studies were maintained under 12:12 h light:dark conditions from 6:00 AM to 6:00 PM. The plasma pharmacokinetics of BMS-

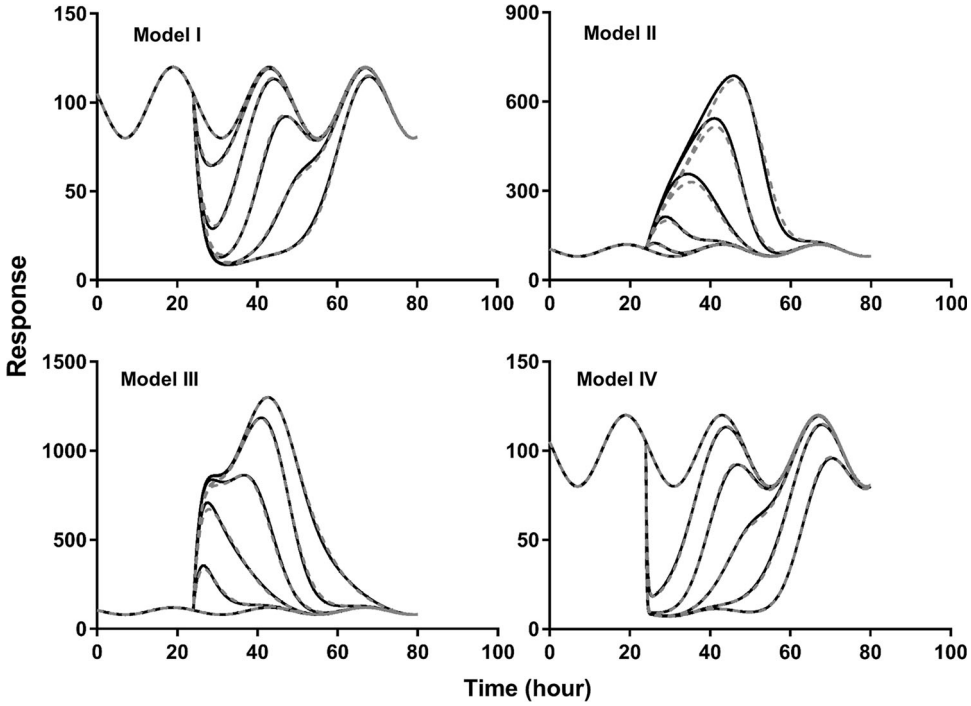

Fig. 2 Model-based simulations of pharmacodynamic response following placebo and doses of 10, 100, 1000, 10,000, and 100,000 mg administered at the mesor of the periodic baseline response. Solid black lines are simulated profiles for baselines with circadian removal $[k_{out}(t)]$ and dashed grey lines for baselines with circadian production rate $[k_{in}(t)]$. Parameter values used for the simulations are listed in the Results

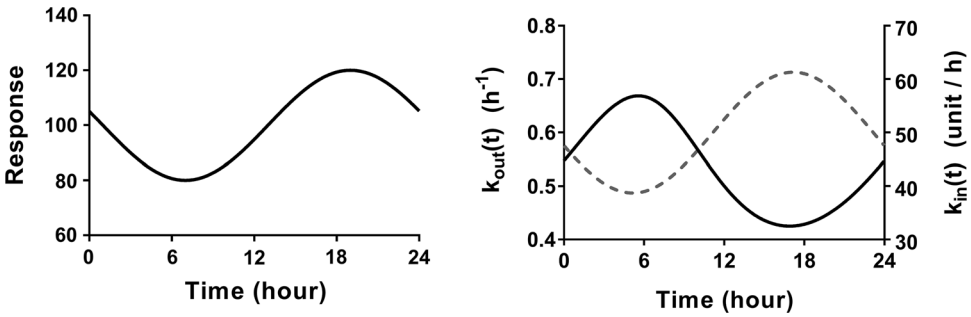

Fig. 3 Model-based simulations of baseline response (left) and underlying turnover process producing rhythmicity in the response variable (right). The periodic behavior of $k_{out}(t)$ is shown on the left y-axis (solid black line) and the periodic behavior of $k_{in}(t)$ is shown on the right y-axis (dashed line)

869780 following 30 and 100 mg/kg oral doses was described by a published one-compartment model using parameter values listed [27]. Since the molecular weight of the compound was not disclosed, simulated plasma drug concentrations are shown in mass rather than in molar units (Fig. 4a). It is assumed that endoproteolytic cellular metabolism produces Aβ with a zero-order rate constant (k_{in}) and Aβ is removed from the interstitium with a time-dependent first-order rate constant $(k_{out}(t))$. In describing the pharmacodynamics, it is assumed that BMS-869780 decreases Aβ in the brain by inhibiting the production rate (k_{in}). The PK/PD model describing the baseline and treatment data is shown in Fig. 4. Depicted in Fig. 4b is the joint characterization of the time courses of brain Aβ at baseline and in response to BMS-869780 at 30 and 100 mg/kg doses. The profile in Fig. 4c shows the characterization of daily variations in baseline brain Aβ in mice. Overlaid on the model-fitted profile are data from placebo-treated mice from the PK/PD study [27]. Circadian variations in the $k_{out}(t)$ is shown by simulation in Fig. 4d. In general, the proposed model jointly captured the baseline and treatment datasets reasonably well. The estimated parameter values are listed in Table 1. A previous study estimated the value of a basic IDR model-derived time-invariant k_{out} for brain $A\beta_{1-42}$ using four separate PK/PD studies in mice as $0.49 \pm 0.11\ h^{-1}$ [28]. The circadian rhythm of the estimated profile of $k_{out}(t)$ is in close agreement with those findings. Estimation of the drug-specific parameter IC_{50} (Table 1), was not significantly perturbed upon assumption of a constant (not shown) versus circadian baseline.

Uricosuric effects

Lesinurad is a selective uric acid reabsorption inhibitor that inhibits the uric acid transporter 1 (URAT1) located in the proximal tubule of the kidney. Through inhibition of URAT1, lesinurad acts as a uricosuric agent, promoting

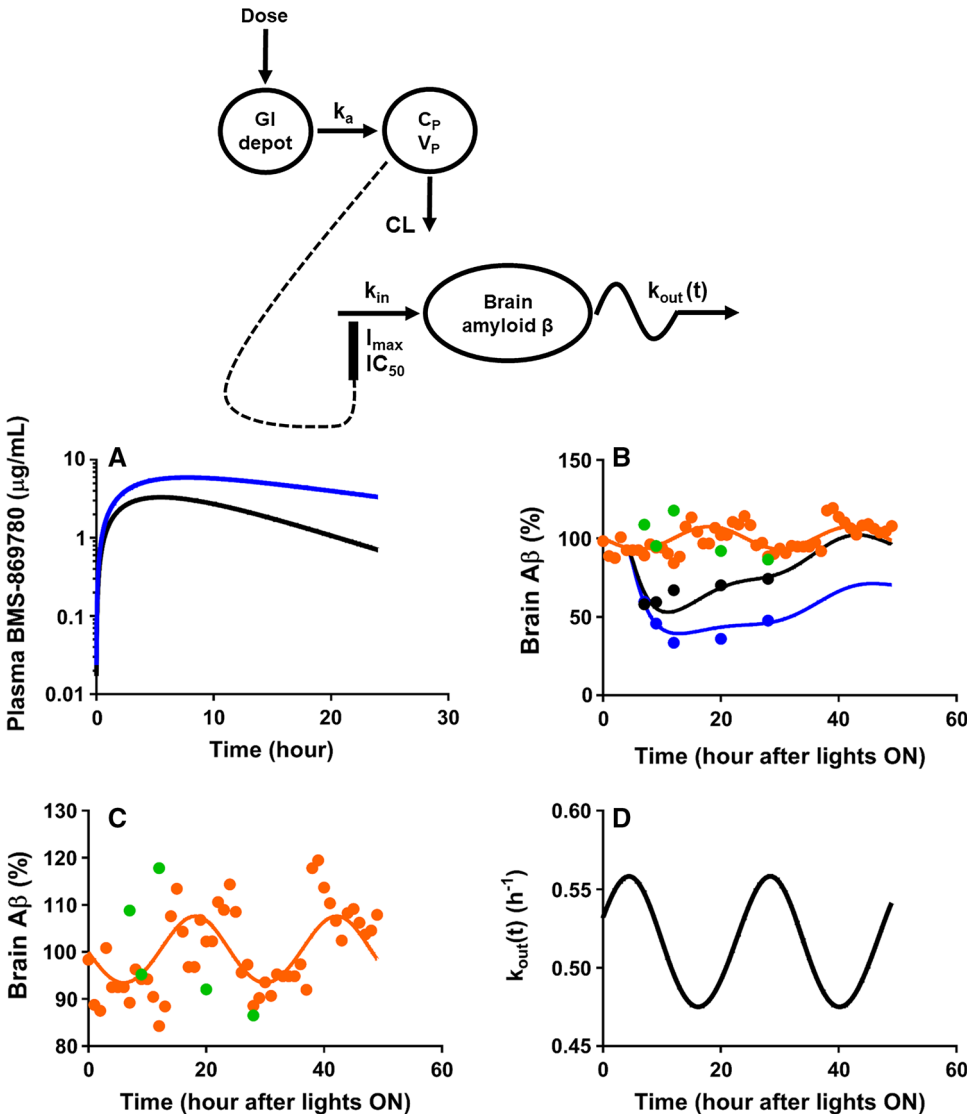

Fig. 4 PK/PD model and profiles for a gamma secretase inhibitor (BMS-869780) on brain amyloid beta in mice. Simulated plasma PK profiles of BMS-869780 (**a**), joint fitting of baseline and treatment data sets (**b**), baseline response of brain amyloid beta (**c**), and simulated $k_{out}(t)$ values (**d**), are shown. The green dots represent placebo data from the treatment studies overlaid on the model fittings (i.e. not included in the model fitting). Symbols represent observed data obtained from Refs. [9] and [27]. Lines are Model I with $k_{out}(t)$ simulated responses. Parameters are presented in Table 1

Table 1 Pharmacokinetic and pharmacodynamic parameters for brain amyloid β suppression by BMS-869780 in mice

Parameter (unit)	Definition	Estimate (% CV)
Pharmacokinetics		
k_{a1}(30 mg/kg) (h^{-1})	Absorption rate constant	0.11[a]
k_{a2} (100 mg/kg) (h^{-1})	Absorption rate constant	0.046[a]
V/F (L/kg)	Volume of distribution	1.94[a]
CL/F (L/h/kg)	Clearance	0.54[a]
Pharmacodynamics		
R_m (%)	Mean baseline (mesor)	100.4 (1.1)
R_a (%)	Amplitude	7.2 (20.5)
T_z (h)	Acrophase	18.1 (4.6)
T (h)	Period	24 (fixed)
k_{in} (% h^{-1})	Zero-order production rate	51.6 (19.5)
I_{max}	Maximal inhibition	1.0 (fixed)
IC_{50} (μg/mL)	Conc. at half-maximal inhibition	3.5 (7.7)

[a]Parameter value fixed from Toyn et al. [26]

uricuresis and thereby lowering serum uric acid [29]. Since lesinurad blocks the reabsorption of uric acid via URAT1 from the tubular fluid into the plasma (response compartment), the model assumed that drug concentrations inhibit a zero-order reabsorption (k_{reabs}) process, while circadian variations in serum uric acid occurs as a function of circadian variations in GFR [23]. To model this time-dependent loss, a mean first-order filtration rate constant (k_{filt}) was calculated using:

$$k_{filt} = \frac{CL_{filtered}}{V_p + V_{ECF}}$$

where V_p is the plasma volume, V_{ECF} is the extracellular fluid volume, and $CL_{filtered}$ is the product of the plasma unbound fraction of uric acid ($f_{u,p}$) and the mesor value of kidney GFR. These parameters were fixed as $f_{u,p} = 0.8$ based on linear binding of uric acid to albumin [30], GFR = 7.2 L/h, V_p = 3 L, and V_{ECF} = 15L. The k_{reabs} constant was assumed to operate under zero-order kinetics and was calculated as the product of the mesor of percent plasma urate and the calculated mesor of k_{filt}. Time-dependent fluctuations in $k_{filt}(t)$ were described using a cosine function which was fitted to baseline and treatment data for plasma uric acid response. The drug was assumed to inhibit k_{reabs}, thereby preventing the reabsorption of uric acid back into the plasma. The final PK/PD model is depicted in Fig. 5.

Data for circadian variations in serum uric acid concentrations in healthy male volunteers under controlled dietary (low-fat) and light/dark conditions were obtained from Sennels et al. [21]. Median concentration and effect data for three dose-escalated treatment arms (100, 200, and

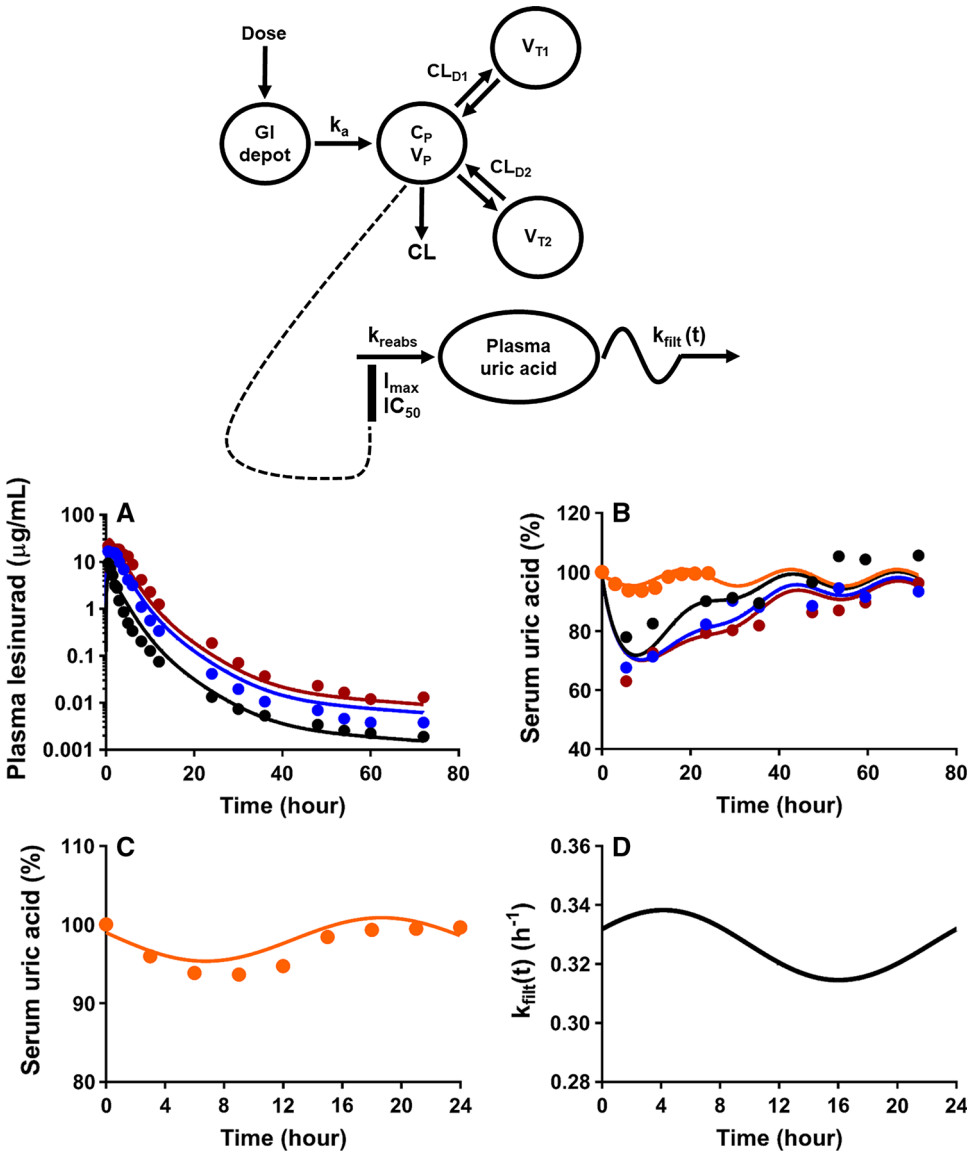

Fig. 5 PK/PD model for uricosuric effects of lesinurad in healthy volunteers. Model fitted plasma PK profiles of lesinurad (**a**), joint fitting of baseline and treatment data (**b**), baseline variations in plasma uric acid (**c**), and simulated $k_{out}(t)$ values (**d**), are shown. Symbols represent observed data obtained from Refs. [21] and [29]. Lines are Model I with $k_{out}(t)$ simulated responses. Parameters are presented in Table 2

Table 2 Pharmacokinetic and pharmacodynamic parameters for the uricosuric effects of lesinurad

Parameter (unit)	Definition	Estimate (% CV)
Pharmacokinetics		
k_a (h^{-1})	Absorption rate constant	3.0 (fixed)
V_P/F (L)	Central volume of distribution	14.7 (12.6)
V_{T1}/F (L)	Peripheral volume of distribution	5.0 (119)
V_{T2}/F (L)	Peripheral volume of distribution	2.4 (37.6)
CL/F (L/h)	Clearance	5.3 (6.7)
CL_{D1}/F (L/h)	Distribution clearance	0.08 (22.9)
CL_{D2}/F (L/h)	Distribution clearance	0.44 (69.1)
Pharmacodynamics		
R_m (%)	Mean baseline (mesor)	98.1 (1.4)
R_a (%)	Amplitude	2.8 (52.3)
T_z (h)	Acrophase	18.7 (8.2)
T (h)	Period	24 (fixed)
k_{in} (% h^{-1})	Zero-order production rate	32 (fixed)
I_{max}	Maximal inhibition	0.29 (7.4)
IC_{50} (μg/mL)	Conc. at half-maximal inhibition	1.02 (32.8)

400 mg oral doses) were digitized from work published by Shen et al. on the pharmacokinetics and uricosuric effects of lesinurad [29]. The data were collected from healthy male subjects. Dosing of subjects was estimated to take place at 9:00 AM. The pharmacokinetics of lesinurad following the three oral doses were simultaneously captured using a three-compartment model with first-order absorption and elimination (Fig. 5a). The characterization of circadian plasma uric acid is shown in Fig. 5b. As depicted in Fig. 5c, the proposed IDR-based model jointly captured the control and treatment data for plasma uric acid humans reasonably well. The simulated profile of $k_{filt}(t)$ (Fig. 5d) resembled the circadian pattern for GFR in healthy subjects [23]. Parameter estimates obtained from model fitting are provided in Table 2. The low estimated I_{max} value of 0.29 (7.4% CV) is attributable to two reasons. First, while lesinurad selectively inhibits URAT1, it is known that other transporters in the renal proximal tubule such as OAT4 are also responsible for the active reabsorption of uric acid [24]. Second, although almost all uric acid is filtered through the glomeruli and over 90% of uric acid is reabsorbed back into the plasma, the major route of production of uric acid in the body is governed by purine metabolism in the liver, which is relatively constant between 300 and 400 mg per day [19].

Inhibition of dopamine reuptake

Dopamine reuptake inhibitors are a frequently used class of drugs used in the treatment of depression, narcolepsy, and attention-deficit hypersensitivity disorder (ADHD). In normal dopaminergic synapses, free dopamine in the synaptic cleft (extracellular fluid) that is not absorbed by the post-synaptic neuron is re-uptaken or recycled by the presynaptic neuron—a process mediated by the dopamine transporter. This mechanism ensures the rapid removal of excess neurotransmitter from the synapse for subsequent neuronal firing. Dopamine reuptake inhibitors act by blocking the dopamine transporter from clearing extracellular dopamine. This results in increased extracellular concentrations of dopamine and an increase in dopaminergic neurotransmission. Circadian oscillations in the activity of the dopamine transporter drives oscillations in extracellular brain dopamine concentrations in mice and rats [17].

Circadian variations in extracellular dopamine over 36 consecutive hours was monitored using brain microdialysis in awake, freely moving adult male Sprague–Dawley rats by Ferris et al. [17]. Raje et al. characterized the concentration–time profile of a benztropines analogue, AHN-1055, in the brain of male Sprague–Dawley rats following a 10 mg/kg IV bolus [31]. The time course of brain AHN-1055 was described by a biexponential equation:

$$C_{brain}(t) = 3599 \cdot e^{-0.42t} + 2193 \cdot e^{-0.11t}$$

Fitting of brain AHN-1055 concentrations is shown in Fig. 6a. The PD effect of a 10 mg/kg IV dose of AHN-1055 on brain extracellular dopamine concentrations in Sprague–Dawley rats was also measured by the same investigators using brain microdialysis [32]. In describing the PD effect of AHN-1055 on dopamine response, it is assumed that presynaptic neurons secrete dopamine at a zero-order rate (k_{in}) with dopamine being cleared from the synapse by a time-dependent removal constant $(k_{out}(t))$. Blockade of dopamine reuptake is assumed to occur via inhibition of $k_{out}(t)$ caused by the drug. The final PK/PD

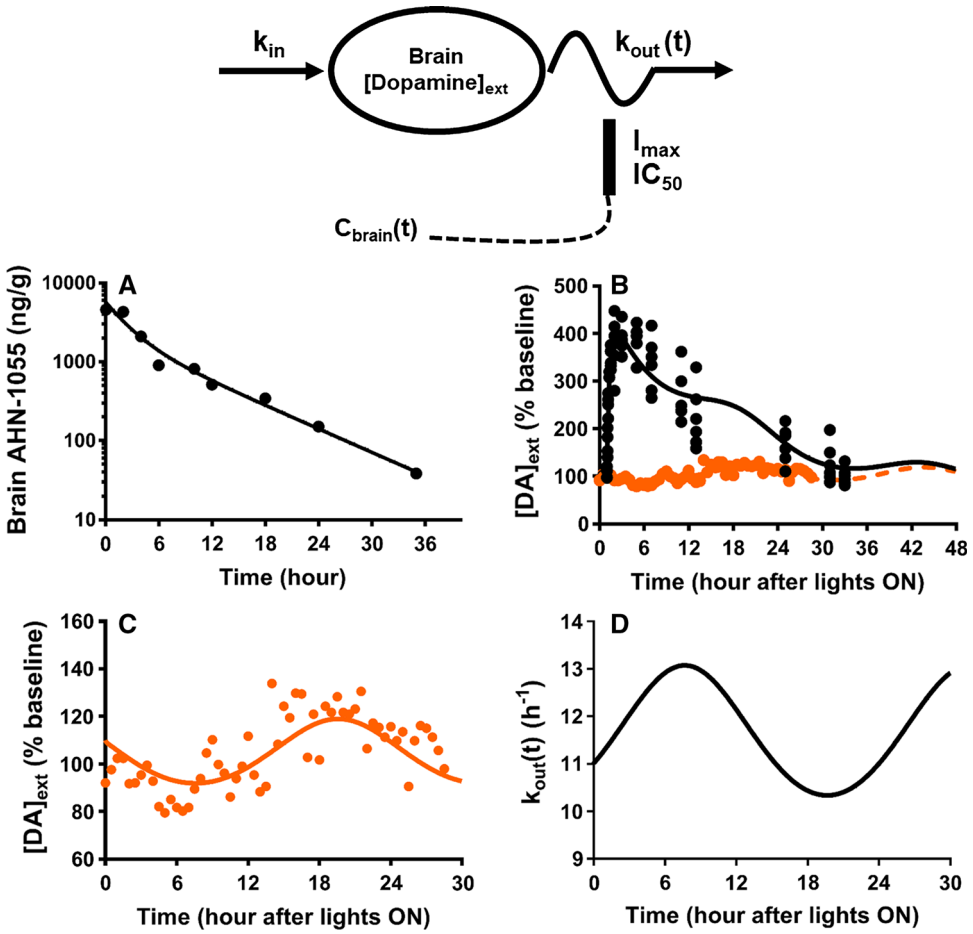

Fig. 6 PK/PD model and effects of a dopamine reuptake antagonist (AHN-1055) on extracellular dopamine in rat brain. Fitted brain PK profile of AHN-1055 (**a**), joint fitting of baseline and treatment data (**b**), circadian variations in brain extracellular fluid (**c**), and simulated $k_{out}(t)$ values (**d**), are shown. Symbols represent observed data obtained from Refs. [17], [31], and [32]. Lines are Model II with $k_{out}(t)$ simulated responses. Parameters are presented in Table 3

model is depicted in Fig. 6. Figure 6b and c present the characterization of the time course of dopamine in the presence and absence of AHN-1055. Shown in Fig. 6d is the profile of $k_{out}(t)$ of brain extracellular dopamine. The times of maximal and minimal rates for circadian dopamine uptake measured in various regions using rat brain slices [17] closely matched peak and nadir of $k_{out}(t)$. Parameter estimates from the model fitting are provided in Table 2. The I_{max} value 0.79 (1.7% CV) and IC_{50} of 145.6 ng/mL (15.1% CV) for AHN-1055 were estimated with reasonable precision. The mesor value of $k_{out}(t)$ was around 12 h^{-1}, which translates to a half-life of extracellular dopamine around 3.4 min. This value is considerably higher than half-life of dopamine elimination from extracellular space in the caudate nucleus (0.2 ± 0.03 s) and prefrontal cortex (1.92 ± 0.22 s) of mice [33].

Discussion

Observations and basic expectations that many endogenous substances may exhibit circadian rhythms resulting from nonstationarity in their removal mechanisms led to this report, which extends the theory and applications of basic indirect response models. The recognition that this type of model may be relevant for endogenous substances is possible upon appreciating that exogenous compounds, when administered at a constant rate (zero-order infusion), can display circadian patterns in their plasma concentrations, such as assessed for 5-fluorouracil [7] and nicotine [34], where circadian metabolism is responsible for their time-dependent patterns. While circadian changes in drug metabolism activity is the major determinant of 5-flurouracil chronopharmacokinetics [8], circadian rhythms in hepatic blood flow [35] limits the clearance of nicotine, a high extraction compound [34]. Similarly, it was expected that a diversity of endogenous substances in the body would display circadian variations arising from non-stationarities in underlying physiological removal mechanisms. Examples of such physiological responses are presented in Figs. 4, 5 and 6.

It is appreciated that circadian rhythmicity in a physiological response can arise either from periodicity in the production rate (k_{in}) or by a period loss rate constant (k_{out}). A well-known example of a circadian physiological response driven by periodic production rates is cortisol

Table 3 Pharmacodynamic parameters for brain extracellular dopamine response following AHN-1055 dosing in rats

Parameter (unit)	Definition	Estimate (% CV)
R_m (%)	Mean baseline (mesor)	104.1 (2.0)
R_a (%)	Amplitude	12.2 (20.9)
T_z (h)	Acrophase	19.7 (3.4)
T (h)	Period	24 (fixed)
k_{in} (% h^{-1})	Zero-order production rate	1202 (11.8)
I_{max}	Maximal inhibition	0.79 (1.7)
IC_{50} (μg/mL)	Conc. at half-maximal inhibition	145.6 (15.1)

secretion [5]. We performed simulations using IDR models with periodic production or loss (Fig. 1) in the absence of drug and across a range of doses to examine possible differences in the resulting signature response profiles. In the absence of any perturbation of the response by drug, it is not possible to identify if the rhythm can be attributed to periodic production or loss, since both models produce identical baseline responses. Dose escalation results only in minute differences in responses driven by circadian k_{in} or k_{out}, and cannot be considered as a technique for mechanism discrimination. As the time of dosing is a factor controlling the magnitude of response, we verified this observation for doses given both at peak and nadir of the baseline.

In addition to fitting the response data shown in Figs. 4, 5 and 6 with the mechanistically appropriate circadian output IDR model, the model fitting of the same data was also performed with use of the circadian input IDR model (not shown). Consistent with expectations based upon the simulations (Fig. 2), model-based discrimination of the applicable $k_{in}(t)$ versus $k_{out}(t)$ mechanism was not possible using standard model selection criteria such as goodness-of-fit plots, residual plots, AIC, and -2LL, since fitting resulted in nearly identical results with both model types (data not shown). The time profiles of underlying $k_{in}(t)$ and $k_{out}(t)$ were, however, markedly different in all of the cases. Therefore, it should be emphasized that the selection of the appropriate circadian model must be based upon knowledge of the mechanisms governing the turnover of the response. Our main purpose was to show how, with an understanding of the underlying physiological mechanisms governing turnover and the mechanism of action of the drugs used, basic processes of periodic production or loss coupled with inhibition or stimulation can govern the time course of pharmacodynamic responses with fluctuating baselines. The examples of the applicable responses discussed in this report were limited to cases where time-course data could be obtained in the literature for responses in the same species under baseline conditions and upon perturbation by drug (collected using similarly controlled study designs). Extensive attempts were made to find suitable PK and PD data in the literature reporting individual values rather than means. However, replicate data (under control and perturbed conditions) of good quality for applicable cases were not found. The IDR model with circadian removal successfully captured the chronobiology and pharmacodynamics of three applicable drug responses, including the uricosuric effects of lesinurad in humans, suppression of the beta amyloid (Aβ) peptide by a gamma-secretase inhibitor in mouse brain, and the modulation of extracellular dopamine by a dopamine transporter inhibitor in rat brain. Other applications of this type of model may extend to the characterization of endogenous substances that are metabolized by enzymes in a circadian manner [36], or the description of rhythms in messenger RNA (e.g. clock genes) [37] or micro RNA [38] that are driven by time-dependent degradation mechanisms at the molecular level.

Recently published by Koch and Schropp [39] were extended IDR models that included a delay process to realize oscillating response behaviors. In their model, production rate was first-order whereas loss was replaced by a second-order term with delayed control by the response variable. Interpretations posited for the delay were lifespan, maturation time, or simply as a necessary parameter [39]. Our current model retained the mathematical properties of the classical IDR model, with a zero-order rate of production but a loss rate constant that changes with time. Periodic changes in the loss constant may be interpreted as underlying circadian variations in the mechanism governing the removal of the response variable, where applicable.

Certain assumptions and limitations exist with use of the proposed IDR models. The current IDR model has been derived for baseline responses assuming cosine behavior. While the cosine function has broad applicability in capturing chronobiologic data, other functions (dual cosines, dual ramp function, or dual zero-order) may offer better description of some oscillating responses. This could have been the case for modeling circadian brain Aβ (Fig. 4c). Nonetheless, the cosine function did reasonably well in describing the circadian response data sets. In dealing with

physiological systems, particularly those with feedback mechanisms, cases can exist where resultant circadian rhythms in the response variable arise from convoluted oscillations in both the production and removal. A good example of such a system would be the homeostatic regulation of glucose and insulin [40, 41]. More detailed experiments would be needed in such instances for deconvolving the contributions of time-dependent production and loss processes. Finally, it is important to verify that time-dependent changes in removal rather than redistribution of substances are responsible for fluctuations in baseline responses before invoking this model.

As demonstrated for other complexities involved with indirect responses [42, 43], this report extends the recognition that the basic indirect response models [2, 3] serve as a starting point in evaluation of relevant pharmacodynamic data and that various physiologic and pharmacologic complexities which complicate the analysis of experimental data can be accounted for within the framework of basic indirect response modeling.

Acknowledgements This work was supported by the National Institutes of Health - National Institute of General Medical Sciences [Grant GM24211].

Appendix

Circadian input

In many pharmacodynamic systems the input rate of measured variables is regulated by endogenous biorhythmic processes such as circadian rhythms [1]. Then k_{in} varies with time $k_{in} = k_{in}(t)$ and consequently the response also exhibits a similar biorhythmic pattern. The simplest biorhythmic response $R_b(t)$ can be described by the cosine function:

$$R_b(t) = R_m + R_a \cos\left(\frac{2\pi}{T}(t - t_p)\right) \tag{13}$$

where R_m is the mean baseline (mesor), R_a is the amplitude ($R_m > R_a$), t_p is the peak time (acrophase), and $T = 24$ h.In the case of a circadian input mechanism, the indirect response model in Fig. 1 is given by

$$\frac{dR_b(t)}{dt} = k_{in}(t) - k_{out} \cdot R_b(t) \tag{14}$$

where $k_{in}(t)$ is circadian function of time and k_{out} is first-order constant. Equation (14) can be re-arranged to express $k_{in}(t)$ as

$$k_{in}(t) = k_{out} \cdot R_b(t) + \frac{dR_b}{dt}(t) \tag{15}$$

Substituting Eqs. (13) into (15),

$$k_{in}(t) = k_{out}R_m + k_{out}R_a cos\left(\frac{2\pi}{T}(t - t_p)\right) + \frac{d}{dt}\left(R_m + R_a cos\left(\frac{2\pi}{T}(t - t_p)\right)\right) \tag{16}$$

Taking the derivative of $\frac{dR_b}{dt}(t)$ in Eq. (16) yields,

$$k_{in}(t) = k_{out}R_m + k_{out}R_a \cos\left(\frac{2\pi}{T}(t - t_p)\right) - \frac{2\pi}{T}R_a \sin\left(\frac{2\pi}{T}(t - t_p)\right) \tag{17}$$

Circadian output

Some mechanisms controlling indirect responses and endogenous markers used in pharmacodynamic modeling can exhibit circadian variations in their rate of removal from the system [1]. Then k_{out} varies with time $k_{out} = k_{out}(t)$. Unlike the case of systems with $k_{in}(t)$, however, the pattern of the circadian response is not expected to follow a biorhythmic pattern similar to $k_{out}(t)$. In the case of a circadian removal mechanism, the indirect response model in Fig. 1 is given by

$$\frac{dR_b(t)}{dt} = k_{in} - k_{out}(t) \cdot R_b(t) \tag{18}$$

where $k_{out}(t)$ is a circadian function of time and k_{in} a zero-order constant. Equation (18) can be re-arranged to express $k_{out}(t)$ as

$$k_{out}(t) = \frac{k_{in} - \frac{dR_b}{dt}(t)}{R_b(t)} \tag{19}$$

Substituting Eq. (13) into (19),

$$k_{out}(t) = \frac{k_{in} - \frac{d}{dt}\left(R_m + R_a \cos\left(\frac{2\pi}{T}(t - t_p)\right)\right)}{R_m + R_a \cos\left(\frac{2\pi}{T}(t - t_p)\right)} \tag{20}$$

Taking the derivative of $\frac{dR_b}{dt}(t)$ in Eq. (20),

$$k_{out}(t) = \frac{k_{in} + \frac{2\pi}{T}R_a \sin\left(\frac{2\pi}{T}(t - t_p)\right)}{R_m + R_a \cos\left(\frac{2\pi}{T}(t - t_p)\right)} \tag{21}$$

References

1. Sukumaran S, Almon RR, DuBois DC, Jusko WJ (2010) Circadian rhythms in gene expression: relationship to physiology, disease, drug disposition and drug action. Adv Drug Deliv Rev 62:904–917

2. Dayneka NL, Garg V, Jusko WJ (1993) Comparison of four basic models of indirect pharmacodynamic responses. J Pharmacokinet Biopharm 21:457–478
3. Jusko WJ, Ko HC (1994) Physiologic indirect response models characterize diverse types of pharmacodynamic effects. Clin Pharmacol Ther 56:406–419
4. Sharma A, Jusko WJ (1998) Characteristics of indirect pharmacodynamic models and applications to clinical drug responses. Br J Clin Pharmacol 45:229–239
5. Chakraborty A, Krzyzanski W, Jusko WJ (1999) Mathematical modeling of circadian cortisol concentrations using indirect response models: comparison of several methods. J Pharmacokinet Biopharm 27:23–43
6. Bruguerolle B (1998) Chronopharmacokinetics. Current status. Clin Pharmacokinet 35:83–94
7. Harris BE, Song R, Soong SJ, Diasio RB (1990) Relationship between dihydropyrimidine dehydrogenase activity and plasma 5-fluorouracil levels with evidence for circadian variation of enzyme activity and plasma drug levels in cancer patients receiving 5-fluorouracil by protracted continuous infusion. Cancer Res 50:197–201
8. Harris BE, Song RL, Soong SJ, Diasio RB (1989) Circadian variation of 5-fluorouracil catabolism in isolated perfused rat liver. Cancer Res 49:6610–6614
9. Roh JH, Huang Y, Bero AW, Kasten T, Stewart FR, Bateman RJ, Holtzman DM (2012) Disruption of the sleep-wake cycle and diurnal fluctuation of beta-amyloid in mice with Alzheimer's disease pathology. Sci Transl Med 4:150ra122
10. Wang Q, Yu X, Li L, Zheng J (2014) Inhibition of amyloid-beta aggregation in Alzheimer's disease. Curr Pharm Des 20:1223–1243
11. Moussa CE (2017) Beta-secretase inhibitors in phase I and phase II clinical trials for Alzheimer's disease. Expert Opin Investig Drugs 26:1131–1136
12. Iliff JJ, Wang M, Liao Y, Plogg BA, Peng W, Gundersen GA, Benveniste H, Vates GE, Deane R, Goldman SA, Nagelhus EA, Nedergaard M (2012) A paravascular pathway facilitates CSF flow through the brain parenchyma and the clearance of interstitial solutes, including amyloid beta. Sci Transl Med 4:147ra111
13. Xie L, Kang H, Xu Q, Chen MJ, Liao Y, Thiyagarajan M, O'Donnell J, Christensen DJ, Nicholson C, Iliff JJ, Takano T, Deane R, Nedergaard M (2013) Sleep drives metabolite clearance from the adult brain. Science 342:373–377
14. Boespflug EL, Iliff JJ (2018) The emerging relationship between interstitial fluid-cerebrospinal fluid exchange, amyloid-beta, and sleep. Biol Psychiatry 83:328–336
15. Tarasoff-Conway JM, Carare RO, Osorio RS, Glodzik L, Butler T, Fieremans E, Axel L, Rusinek H, Nicholson C, Zlokovic BV, Frangione B, Blennow K, Menard J, Zetterberg H, Wisniewski T, de Leon MJ (2016) Clearance systems in the brain—implications for Alzheimer disease. Nat Rev Neurol 12:248
16. Castaneda TR, de Prado BM, Prieto D, Mora F (2004) Circadian rhythms of dopamine, glutamate and GABA in the striatum and nucleus accumbens of the awake rat: modulation by light. J Pineal Res 36:177–185
17. Ferris MJ, España RA, Locke JL, Konstantopoulos JK, Rose JH, Chen R, Jones SR (2014) Dopamine transporters govern diurnal variation in extracellular dopamine tone. Proc Natl Acad Sci USA 111:E2751–E2759
18. Sleipness EP, Sorg BA, Jansen HT (2007) Diurnal differences in dopamine transporter and tyrosine hydroxylase levels in rat brain: dependence on the suprachiasmatic nucleus. Brain Res 1129:34–42
19. Maiuolo J, Oppedisano F, Gratteri S, Muscoli C, Mollace V (2016) Regulation of uric acid metabolism and excretion. Int J Cardiol 213:8–14
20. So A, Thorens B (2010) Uric acid transport and disease. J Clin Invest 120:1791–1799
21. Sennels HP, Jorgensen HL, Goetze JP, Fahrenkrug J (2012) Rhythmic 24-h variations of frequently used clinical biochemical parameters in healthy young males—the Bispebjerg study of diurnal variations. Scand J Clin Lab Invest 72:287–295
22. Yu KH, Luo SF, Tsai WP, Huang YY (2004) Intermittent elevation of serum urate and 24-h urinary uric acid excretion. Rheumatology 43:1541–1545
23. Koopman MG, Koomen GC, Krediet RT, de Moor EA, Hoek FJ, Arisz L (1989) Circadian rhythm of glomerular filtration rate in normal individuals. Clin Sci (Lond) 77:105–111
24. Diaz-Torne C, Perez-Herrero N, Perez-Ruiz F (2015) New medications in development for the treatment of hyperuricemia of gout. Curr Opin Rheumatol 27:164–169
25. D'Argenio D, Schumitzky A, Wang X (2009) ADAPT 5 User's Guide: Pharmacokinetic/pharmacodynamic Systems Analysis Software. BioMedical Simulations Resource, Los Angeles
26. Sun YN, Jusko WJ (1999) Role of baseline parameters in determining indirect pharmacodynamic responses. J Pharm Sci 88:987–990
27. Toyn JH, Thompson LA, Lentz KA, Meredith JE Jr, Burton CR, Sankaranararyanan S, Guss V, Hall T, Iben LG, Krause CM, Krause R, Lin XA, Pierdomenico M, Polson C, Robertson AS, Denton RR, Grace JE, Morrison J, Raybon J, Zhuo X, Snow K, Padmanabha R, Agler M, Esposito K, Harden D, Prack M, Varma S, Wong V, Zhu Y, Zvyaga T, Gerritz S, Marcin LR, Higgins MA, Shi J, Wei C, Cantone JL, Drexler DM, Macor JE, Olson RE, Ahlijanian MK, Albright CF (2014) Identification and preclinical pharmacology of the gamma-secretase modulator BMS-869780. Int J Alzheimers Dis 2014:431858
28. Lu Y, Barton HA, Leung L, Zhang L, Hajos-Korcsok E, Nolan CE, Liu J, Becker SL, Wood KM, Robshaw AE, Taylor CK, O'Neill BT, Brodney MA, Riddell D (2013) Cerebrospinal fluid beta-amyloid turnover in the mouse, dog, monkey and human evaluated by systematic quantitative analyses. Neurodegener Dis 12:36–50
29. Shen Z, Rowlings C, Kerr B, Hingorani V, Manhard K, Quart B, Yeh LT, Storgard C (2015) Pharmacokinetics, pharmacodynamics, and safety of lesinurad, a selective uric acid reabsorption inhibitor, in healthy adult males. Drug Des Devel Ther 9:3423–3434
30. Campion DS, Bluestone R, Klinenberg JR (1973) Uric acid: characterization of its interaction with human serum albumin. J Clin Invest 52:2383–2386
31. Raje S, Cao J, Newman AH, Gao H, Eddington ND (2003) Evaluation of the blood-brain barrier transport, population pharmacokinetics, and brain distribution of benztropine analogs and cocaine using in vitro and in vivo techniques. J Pharmacol Exp Ther 307:801–808
32. Raje S, Cornish J, Newman AH, Cao J, Katz JL, Eddington ND (2005) Pharmacodynamic assessment of the benztropine analogues AHN-1055 and AHN-2005 using intracerebral microdialysis to evaluate brain dopamine levels and pharmacokinetic/pharmacodynamic modeling. Pharm Res 22:603–612
33. Yavich L, Forsberg MM, Karayiorgou M, Gogos JA, Mannisto PT (2007) Site-specific role of catechol-*O*-methyltransferase in dopamine overflow within prefrontal cortex and dorsal striatum. J Neurosci 27:10196–10209
34. Gries JM, Benowitz N, Verotta D (1996) Chronopharmacokinetics of nicotine. Clin Pharmacol Ther 60:385–395
35. Lemmer B, Nold G (1991) Circadian changes in estimated hepatic blood flow in healthy subjects. Br J Clin Pharmacol 32:627–629

36. Levi F, Schibler U (2007) Circadian rhythms: mechanisms and therapeutic implications. Annu Rev Pharmacol Toxicol 47:593–628
37. Sukumaran S, Xue B, Jusko WJ, DuBois DC, Almon RR (2010) Circadian variations in gene expression in rat abdominal adipose tissue and relationship to physiology. Physiol Genomics 42A:141–152
38. Heegaard NHH, Carlsen AL, Lilje B, Ng KL, Rønne ME, Jørgensen HL, Sennels H, Fahrenkrug J (2016) Diurnal variations of human circulating cell-free micro-RNA. PLoS One 11:e0160577–e0160577
39. Koch G, Schropp J (2018) Delayed logistic indirect response models: realization of oscillating behavior. J Pharmacokinet Pharmacodyn 45:49–58
40. Sukumaran S, Jusko WJ, DuBois DC, Almon RR (2011) Mechanistic modeling of the effects of glucocorticoids and circadian rhythms on adipokine expression. J Pharmacol Exp Ther 337:734–746
41. Boden G, Ruiz J, Urbain JL, Chen X (1996) Evidence for a circadian rhythm of insulin secretion. Am J Physiol 271:E246–252
42. Krzyzanski W, Chakraborty A, Jusko WJ (2000) Algorithm for application of Fourier analysis for biorhythmic baselines of pharmacodynamic indirect response models. Chronobiol Int 17:77–93
43. Krzyzanski W, Jusko WJ (2001) Indirect pharmacodynamic models for responses with multicompartmental distribution or polyexponential disposition. J Pharmacokinet Pharmacodyn 28:57–78